J. Eng. Technol. Sci., Vol. 53, No. 2, 2021, 210211

Corrosion Assessment of Pre-corrosion Concrete Specimens using Acoustic Emission Technique

Ahmad Zaki[1,*] & Zainah Ibrahim[2]

[1]Department of Civil Engineering, Faculty of Engineering, Universitas Muhammadiyah Yogyakarta, Bantul, 55183 Daerah Istimewa Yogyakarta, Indonesia
[2]Department of Civil Engineering, Faculty of Engineering, University of Malaya, 50603 Kuala Lumpur, Malaysia,
*E-mail: ahmad.zaki@umy.ac.id

Highlights:

- The , RA and AF of AE parameters were useful in association with fracture mechanisms of pre-corroded beam specimens.
- The damage of corroded RC beam specimens were sufficiently characterized by the cumulative AE hits.
- Loss of cross-section (mass loss) was a factor that contributed to loss of strength due to steel corrosion in concrete specimens.

Abstract: The acoustic emission (AE) technique is known as a non-destructive testing (NDT) method, which is effective for assessing corrosion in concrete structures. This study aims to utilize the AE technique, for the assessment of pre-corroded concrete specimens, which are under load testing. Experiments were carried out on small-scale pre-corroded specimens, which were subjected to monotonic loading. The results showed that the majority of the beam specimens failed with shear cracks. Three AE parameters, namely acoustic emission hits, as well as the RA and AF values, were also used, in order to assess the flexure behaviour of the pre-corroded beam specimens. These experiments helped to understand the flexural behaviour of pre-corroded specimens, which were under a loading test, via the use of the AE technique.

Keywords: *AE; corrosion; concrete; flexural behaviour; NDT.*

1 Introduction

The acoustic emission (AE) technique is known as a non-destructive testing (NDT) method, which is useful in assessing steel corrosion in reinforced concrete (RC) structures. This is due to its capability to detect steel corrosion. The AE technique also monitors and analyzes energy signals successfully, due to the corrosion of steel reinforcements by acoustic emission sensors, which are placed on the surface of the concrete. Also, AE parameters such as AEhits, energy, and signal strength, are used to characterize the corrosion process in steel reinforcements [1-8]. The sources of the AE are classified into two forms, namely

Received December 13th, 2019, Revised August 13th, 2020, Accepted for publication March 15th, 2021.
 ISSN: 2337-5779,
DOI: 10.5614/j.eng.technol.sci.2021.53.2.11

average frequency (AF) and RA value, which are both used in order to distinguish between the failure types. Besides, AE amplitude parameters, such as the *b-value* and *I*b-values, have also been proposed for assessing damage severity in RC structures [4, 9-14]. Furthermore, the AE technique enables damage localization of steel corrosion, as well as the detection of micro and macro cracking [15-17]. This research aims to use AE technique in monitoring pre-corroded concrete specimens, which are subjected to flexural loading. Moreover, three parameters, AE hits, as well as the AF and RA values, are to be used, in order to characterize the corrosion damage of pre-corroded specimens.

2 Corrosion Assessment Using AE Technique

In the field of civil engineering, the AE technique has been widely used for structural health monitoring (SHM) and assessment of steel corrosion damage, especially in the evaluation of corroded concrete structures [6, 7, 18-22]. This AE technique was operated without disturbances to the processes and progressions associated with concrete structures [23-26]. The first study of this technique was carried by Dunn, *et al.* [27], in order to assess corrosion in a series of laboratory tests . The AE technique is also applicable, feasible, and sensitive, when analyzing and monitoring steel corrosion in RC structures. Moreover, there are two types of AE data measurement, namely parameter and signal-based analysis [26, 28, 29]. The principle of the AE technique is shown in Figure 1.

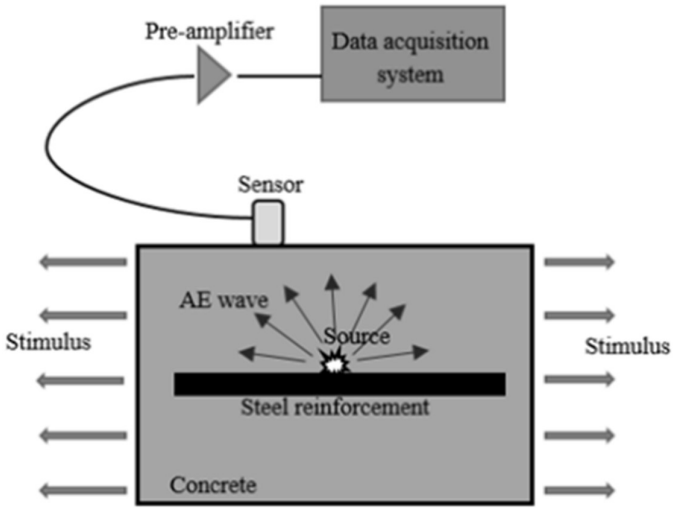

Figure 1 Acoustic emission technique [30,31].

3 Corrosion Assessment Using AE

3.1 Accelerating of Steel Corrosion

Figure 2 below shows the accelerated corrosion process of the steel reinforcements. In this process, steel reinforcements with a size of 12 mm in compliance with BS 4449 [32], was used as a tension reinforcement. These steel reinforcements were immersed into a 5% sodium chloride (NaCl) solution in a plastic container, and were corroded before concrete casting. Also, a direct current (DC) power supply was used for electrolysis, as the steel reinforcement was connected to the positive terminal, at the anode. However, the steel reinforcement bar was connected to the negative terminal at the cathode.

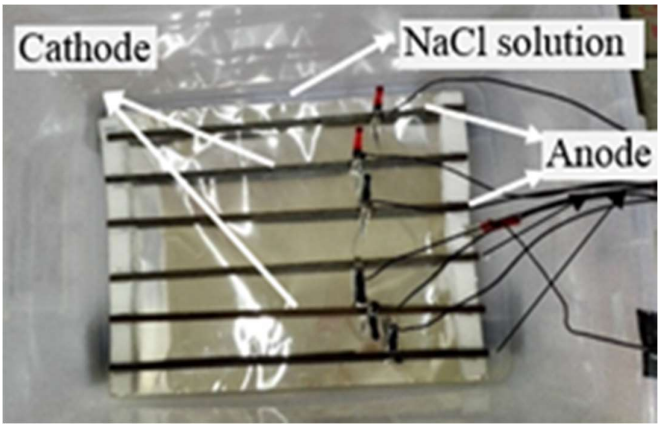

Figure 2 Accelerated steel corrosion.

Therefore, after the corrosion process, the product (rust) on the steel reinforcements was removed, in accordance with ASTM G1-03 [33]. The corroded steel reinforcement was then weighed, in order to assess the mass loss.

3.2 Assessing Steel Corrosion

Based on converting the current flow, the mass loss was determined though the use of Faraday's law, as shown in Eq. (1),

$$\Delta m = \frac{M.I.t}{z.F}\frac{M.I.t}{z.F}, \tag{1}$$

where,

Δm = steel consumed (g, gram)
M = atomic weight of metal (56 g/mol for steel)
I = current (A, amperes)

t = time current (s, seconds)
z = ionic charge or electrons transferred in the half-cell reaction (2 for steel)
F = Faraday's constant (96500 A/s)

3.3 Fabrication of Concrete Specimens

Six pre-corroded specimens with dimensions of 100 x 100 x 500 mm^3 were reportedly fabricated in this process. The details of these pre-corroded specimens are shown in Figure 3.

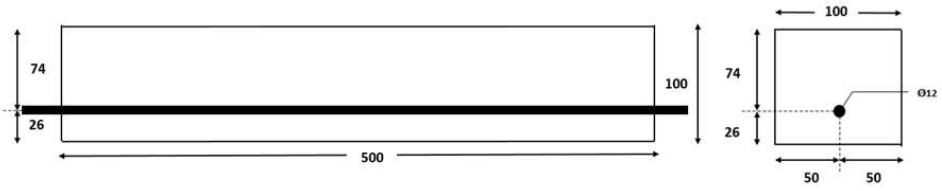

Figure 3 Beam specimens (in mm).

In accordance with BS 8110-1, beam specimens with 28 MPa of compressive strength were produced in one batch of concrete casting [34]. The dry density of concrete was 2192.91 kg/m^3, as the beam specimens (with steel reinforcements) having corrosion levels of 0%, 8.17%, 9.06%, 24.21%, 27.56%, and 50.57%, were prepared as pre-corrosion samples. The corrosion level (%) of the beam specimens was also measured as the mass loss of steel reinforcement, before and after accelerated testing of steel corrosion [35, 36]. Moreover, the bottom cover was also located at 26 mm from the concrete surface. Ordinary Portland cement (OPC), river sand, and crushed-type granite (with a maximum aggregate size of 10 mm) were also used in preparing the concrete specimens.

3.4 Data Acquisition

The pre-corroded specimens were subjected to a three-point load testing. The flexural load test was carried out using a universal testing machine (INSTRON Satec Series) at 100 kN, as shown in Figure 4. Each specimen was also supported at both ends, with the distance between the supports and loading point being 200 mm.

Furthermore, data acquisition from the pre-corroded specimens was conducted using the AE technique, throughout the flexural load testing. A PCI-2 AE System from MITRAS Group, Inc., was observed to be connected to six acoustic emission sensors, which were mounted on the surface of the specimens, via the use of wax as a coupling agent.

Figure 4 Data acquisitions using an INSTRON Satec Series universal testing machine at 100 kN and AE technique.

4 Results and Discussion

4.1 Compressive Strength and Modulus Elasticity

Table 1 below, showed the compressive strength and average modulus from the elasticity tests, which were carried out on the casted concrete samples in the experiment. As indicated in Table 1, compressive strength on the 7th and 28th day was observed to be higher than the design strength of 28 MPa. However, the concrete had already met its characteristic strength on the 7th day. Besides that, the modulus of elasticity was 26.49 GPa.

Table 1 Compressive strength and average modulus of elasticity of concrete.

Age of concrete	Compressive strength (MPa)		Average modulus of elasticity (GPa)
	For one specimen	Average	
7th day	30.85	29.40	-
	27.11		
	30.25		
28th day	35.14	37.31	26.49
	37.79		
	38.99		

4.2 Corrosion Level

After the accelerated corrosion test via the impressed current technique, the steel reinforcements were cleaned, in order to remove the rust. The results after cleaning are shown in Figure 5.

Also, Table 2 indicated the quantitative results, as six steel reinforcements casted into the beam specimens with corrosion levels between 0–51%, were used in the experiment.

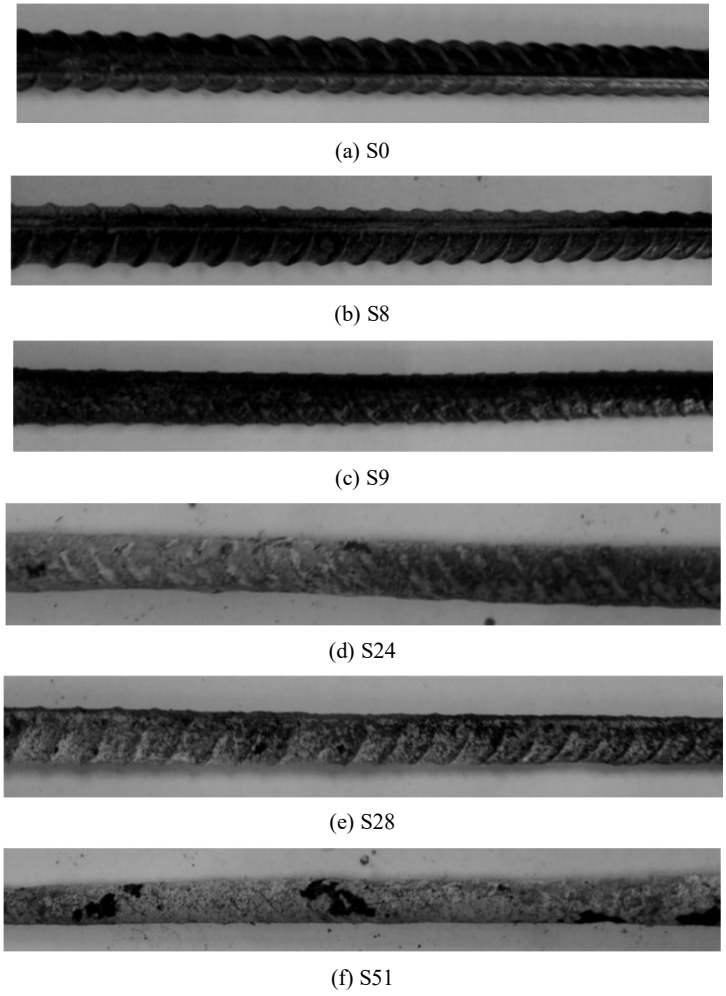

(a) S0

(b) S8

(c) S9

(d) S24

(e) S28

(f) S51

Figure 5 Condition of steel reinforcements after accelerated corrosion test.

Table 2 Quantitative results of accelerated corrosion process.

Beam specimens	Initial mass, M_i (g)	Final mass, M_f (g)	Mass loss, Δm (g)	Corrosion level (%)
S0	520	520	0	0.00
S8	514	472	42	8.17
S9	508	462	46	9.06
S24	504	382	122	24.21
S28	508	368	140	27.56
S51	522	258	264	50.57

4.3 Mechanical Behaviour

Figure 6 showed that most of the beam specimens in this research had experienced brittle failure. Also, the specimen with the highest level of corrosion (i.e. S51) was observed to have experienced significant yielding (before failure), which further indicated ductile failure. Theoretically, the S0 beam specimen should have experienced ductile failure, which indicated that the section was still under-reinforced.

The steel reinforcements was also observed to have attained its yield strength, compared to the concrete. As the steel reinforcement started to yield, the beam began to sag, and large tensile cracks became visible, before eventually failing. Therefore, the S0 beam specimen experienced brittle failure. According to observations, the S0 beam specimen suddenly failed, with the concrete also failing in compression. This mode of failure was not preferable, as it provided little or no warning before its occurrence. Therefore, this failure mode was observed to have low safety.

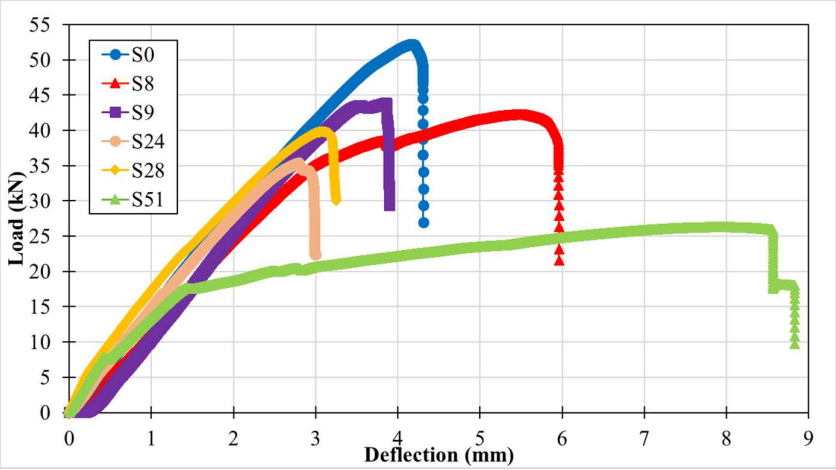

Figure 6 Load versus deflection of the beam specimens.

However, as corrosion levels increased, there was a shift in the dominant failure mode from brittle to ductile, as shown in Figure 6. The yield of steel reinforcements became more pronounced with the increment of the corrosion level, inferring the higher working stress sustained, as a result of the effective cross sectional area reduction.

By plotting the peak load against corrosion level, a linear increase was found with the decreasing load capacity of the pre-corroded specimens, as shown in Figure 7. The regression value (R^2) of the linear graph with a negative gradient was 0.934, which was very acceptable due to being close to 1. Additionally, this result confirmed that the beam specimen's capacity loss was linked with that of the cross-section, at the failure location.

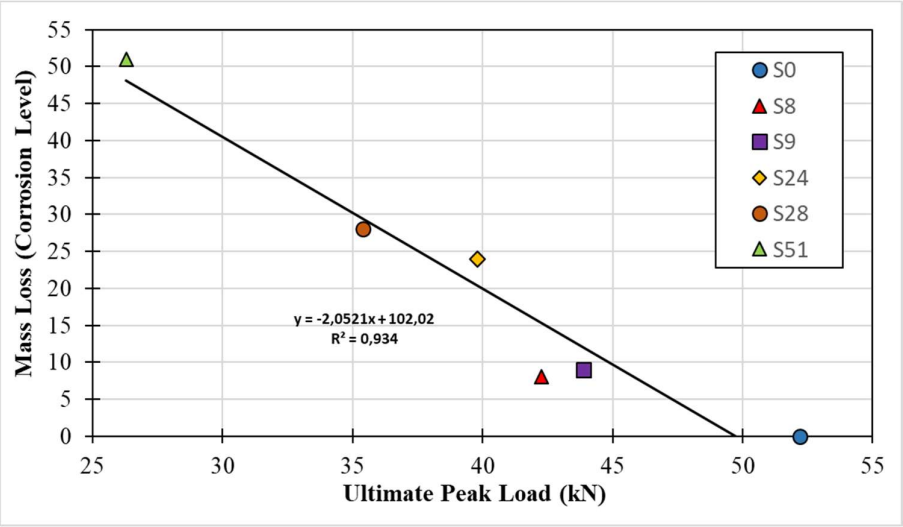

Figure 7 Loss of ultimate strength vs. mass loss of the beam specimens.

Furthermore, Figure 8 indicated that majority of the specimens had failed, due to shear and small cracks at the support and middle part of the beams. However, specimen S51, which had the highest level of corrosion, failed in the middle part of the beam, with a single crack.

As the loading process progressed, a crack started to develop at the support, which propagated further to the top of the middle span with an increase in width, until the occurrence of failure. Moreover, the crack formation in the S51 specimen was probably due to the reduced cross section of the steel reinforcement, as well as the existence of corrosion pits, which acted as precursors to cracking.

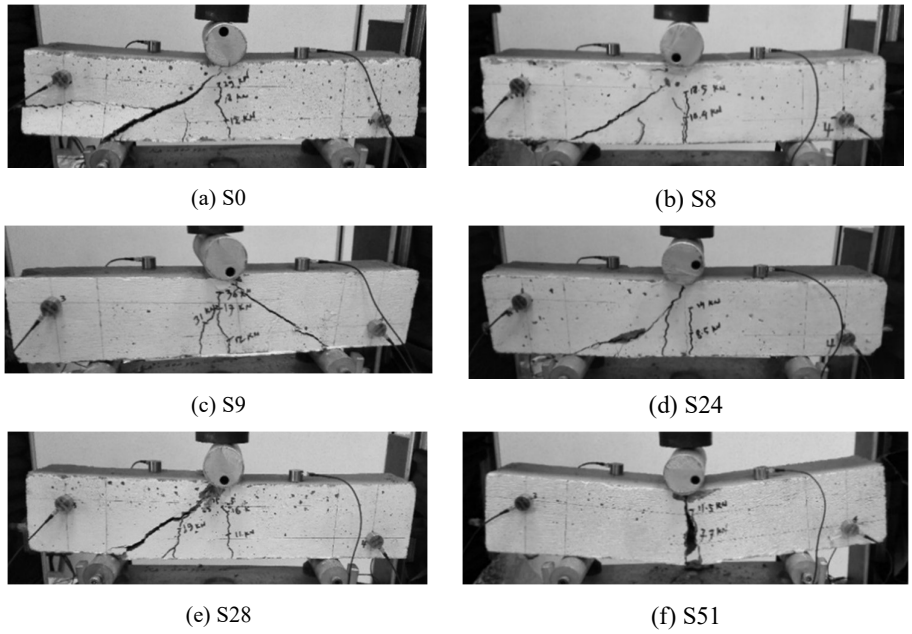

(a) S0 (b) S8

(c) S9 (d) S24

(e) S28 (f) S51

Figure 8 Condition of the specimens after failure.

Based on the load and deflection curves as well as observations, the development of the beam damage was classified into three general levels, as shown in Figure 6. These classification includes damage level 1 (micro-cracking), 2 (first visible crack and crack distribution), and 3 (damage classification), which were further represented as DL1, DL2, and DL3, respectively.

4.4 AE Technique Data

4.4.1 Cumulative AE Hits

Based on Figure 9, the cumulative AE hits and load level (%) of the pre-corroded specimens were indicated. Generally, the cumulative AE hits were observed to increase as the level of specimens' corrosion also improved, due to the loss of cross section. However, the corrosive beam specimens (S8, S9, S24, S28, and S51) experienced different trends of cumulative AE hits. This was due to the presence of different levels of corrosion pits in the steel reinforcements, which resulted into high AE activity in the beam specimens.

When the load was applied, the AE hits also increased, prior to the appearance of the first visible crack. After the first cracking of the concrete between 10 to 20% of the load level, the AE hit level was observed to have significantly increased.

Afterwards, the cracks was found to have propagated, as the AE hits gradually increased until the failure of the beam specimen, during the loading process. However, for the S9 specimen, the AE hit activity increased insignificantly (stagnant) at around 2 x 10^5, after a load level of 50%. This occurrence was probably due to stressing and concrete cracking, especially the longitudinal type near the steel reinforcement, which was dissipated due to corrosion.

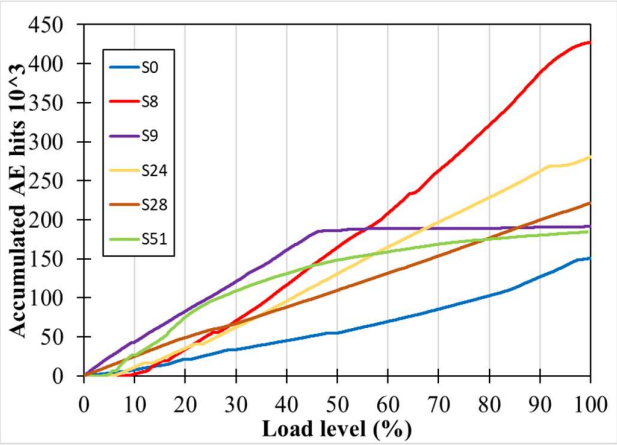

Figure 9 Cumulative AE hits versus load level (%) of the specimens.

4.4.2 Crack Classification – RA Value and AF

In order to study the mechanism of the pre-corroded specimens' fracture in a more detailed way, the RA value and the average frequency (AF) were plotted against load (kN), as shown in Figure 10. From the beginning of the loading process in the S0 specimen, shear cracks were observed due to high RA and low AF values [17, 37]. This indicated that high-density events occurred within the concrete in the tension area [8]. Moreover, after the first few loads until the end of damage level 1 (when the first visible crack occurred), the RA and AF values significantly decreased and increased, respectively.

This indicated that micro-fractures were extensively propagated. After the first visible crack occurred, the RA and AF values tended to increase and decrease, respectively, therefore, resulting in the occurrence of shear cracking. This also indicated the nucleation of the concrete cracking. After 17 kN of this load, both the RA and AF values fluctuated, therefore resulting in the occurrence of a shear and tensile cracking. During the early phase of damage level 3, which occurred slightly after yielding, the increase and decrease of the RA and AF values suggested shear cracking, respectively. This indicated the progress of concrete cracking, due to ultimate failure.

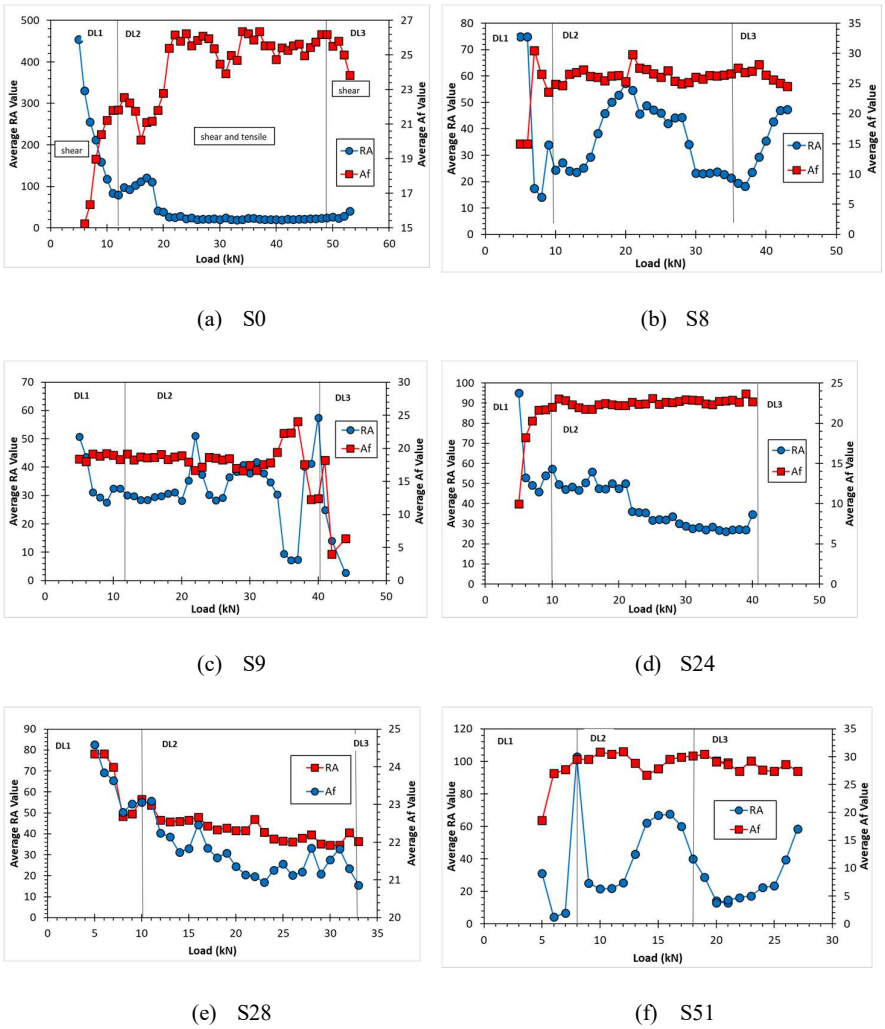

(a) S0 (b) S8

(c) S9 (d) S24

(e) S28 (f) S51

Figure 10 Average RA and AF values versus load of the specimens.

Furthermore, all the corroded beams specimens (i.e. S8, S9, S24, S28, and S51) showed similar trends, as the S0 sample was different at damage level 1. However, after the first visible crack of the S28 specimen, both the RA and AF values fluctuated until the end of the loading process. This indicated the even occurrence of shear and tensile cracking, until the ultimate failure of the concrete specimen. Meanwhile, when the first crack occurred at the S51 pre-corroded

specimen, a sudden increase in the values of RA & AF was detected, which indicated the occurrence of tensile cracking.

This condition also showed the occurrence of macro-fractures in the tensile reinforcement area. Moreover, the significant pitting corrosion occurred at the middle part of the steel reinforcements. This pitting corrosion is also known to help tensile cracks propagate extensively. At damage level 2, a mixture of tensile and shear cracking occurred, as well as a significant increase and decrease in the values of RA & AF, respectively. There was also shear cracking in the tensile area, due to the extensive yield of the steel reinforcement. After the yielding point, which was at damage level 3, the beam specimen had tensile cracks, due to a decrease in the RA and AF values. However, at the end of the damage level 3, the relationship switched to shear cracking. Before the failure of the concrete beam, the RA and AF values significantly increased and decreased, respectively. This phenomenon was found to be associated with the yielding of the steel reinforcement, until it breaks into two parts.

Aggelis, *et al*. [17], explained that the wave modes were often excited by crack type (i.e. shear or tensile cracks). Even though longitudinal waves were still excited, most of the energy transmitted were shear waves, which were slower. Due to this, most of the energy (or maximum amplitude) arrived later than the first longitudinal wave, therefore, resulting in a high RA value. However, tensile cracks were observed to cause a transient volumetric change inside the material, as well as convert the released energy into longitudinal (dilatational) waves. Therefore, the excited pulses containing longitudinal waves of large amplitude, were faster than other types of crack, with the resulting RA value being low. Based on Figure 11, it was observed that, as the corrosion level became higher, the average AF and RA values increased and decreased, respectively.

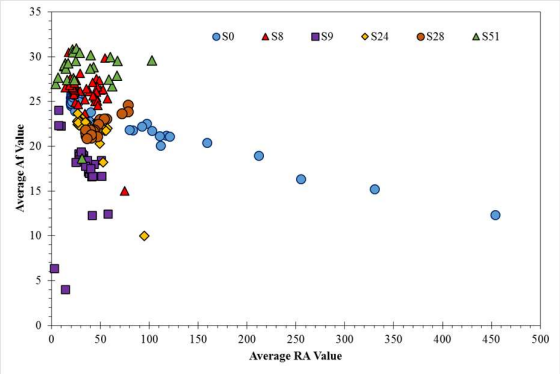

Figure 11 Average AF against average RA value.

4.4.3 *I*b-value

Before and after filtering, the *I*b-value of the S0 beam specimen was shown in Figure 12. During this process, the Savitzky-Golay smoothing method was used, in order to filter the *I*b-values of the beam specimen. The filter had two options for parameter filtering, namely polynomial fit (N) and window length (F). This filter was also suitable for a variable that was slowly varying and corrupted by random noise.

In order to smoothen the noisy parameters, the replacement of each data point was beneficial to the signal-to-noise ratio increase, without even distorting the signal. Moreover, averaging was found to reduce the level of noise without influencing the value obtained. This was due to nearby points being measured close to the same underlying value.

Furthermore, Figures 12(b) and 13, showed the filtered *I*b-values for the six beam specimens. The solid line described the trend of the *I*b-value, as it was clearly observed that all the beam specimens displayed a similarities, except for the S51 sample, with a corrosion level of 51%. For the S0 beam specimen, the trend established was due to an increase in the *I*b-value during damage level 1, which was further accompanied by a slight fluctuation and decrease in DL2 & DL3, respectively.

This indicated that micro-crack formation was dominant before the first crack that occurred during damage level 1, due to a steady rise of the *I*b-value. Immediately the first crack occurred at damage level 2, the localization of macro-cracks began. At the damage level 3, the *I*b-value was observed to have decreased, due to macro cracks starting to open. Also, the decreasing trend of the Ib-value was observed as a serious damage alert.

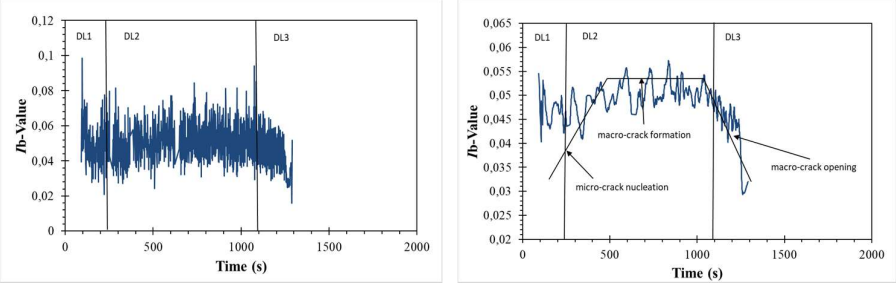

(a) Before filtering (b) After filtering

Figure 12 Ib-value of the S0 beam specimen.

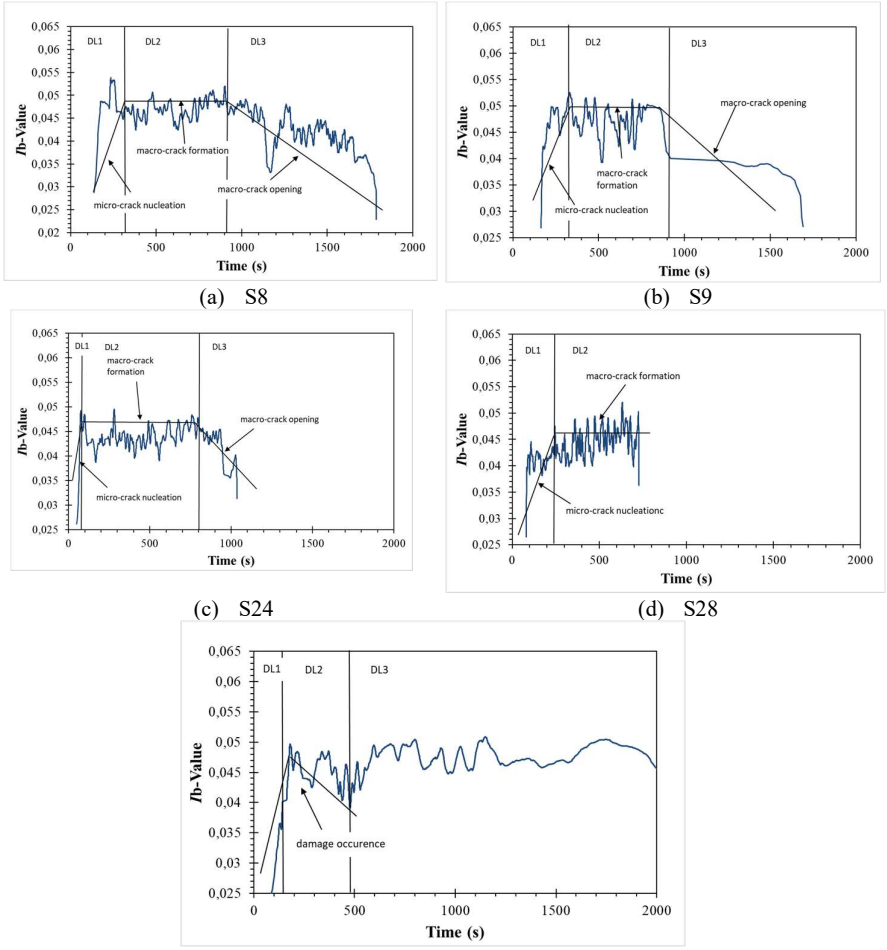

(a) S8 (b) S9

(c) S24 (d) S28

(e) S51

Figure 13 *Ib*-value against time of the beam specimens.

With the exception from other specimens, the S51 sample (highest corrosion level) showed a significant drop in *I*b-value, at the early phase of damage level 2. The drop of this Ib-value indicated the occurrence of damage. Also, the cross section reduction due to corrosion, caused cracks to open in the tension reinforcement area of the beam specimen. When the first visible crack occurred in the early phase of damage level 2, the *I*b-value decreased until the inception of DL3. Moreover, this continued to fluctuate, until the failure of the beam specimen. This indicated that after the first visible crack, macro-cracks were observed to be propagated until the occurrence of failure.

5 Conclusions

The conclusions based on the results obtained from the testing of pre-corroded beam specimens under flexure loading, was summarized as follows,

1. Majority of the beam specimens were observed to have failed with shear cracks. However, the specimen with the highest level of corrosion failed with tensile cracks. This was probably due to cross section losses of the steel reinforcement, as well as the existence of pitting corrosion, which acted as precursors to cracking.
2. The AE parameters, such as the RA and AF values, were useful in the association with fracture mechanisms of pre-corroded beam specimens. Shear cracks were also observed due to a high RA and low AF values at damage level 1. This result indicated that high-intensity events occurred within the concrete in the tension reinforcement area, due to corrosion.
3. The damage of the corroded RC beam specimens was sufficiently characterized by the cumulative AEhits and *I*b-value in the AE data. In the pre-corrosion beam specimens, the cumulative AE hits increased in correlation with the corrosion level of the steel reinforcements. This was due to the presence of pitting corrosion in the steel reinforcements, which caused high AE activity. Furthermore, the *I*b-value increased during damage level 1, accompanied by a slight fluctuation and decrease in the *I*b-values, in DL2 & DL3, respectively. A decreasing trend in the *I*b-value was also considered to be a serious damage alert.
4. The loss of cross-section (mass loss) was a factor that contributed to the loss of strength by steel corrosion in beam specimens. Also, the increased level of corrosion in the steel reinforcements was found to have a linear relationship with the decreasing load capacity of the corroded beam specimens.

Nomenclature

AE	=	acoustic emission
NDT	=	non-destructive testing
RC	=	reinforced concrete
AF	=	average frequency
SHM	=	structural health monitoring
NaCl	=	sodium chloride
DC	=	direct current
Δm	=	mass loss
M	=	atomic weight of metal
I	=	current
t	=	time
z	=	ionic charge or electrons transferred in the half-cell reaction (2 for steel)
F	=	Faraday's constant

References

[1] Yoon, D.J., Weiss, W.J. & Shah, S.P., *Assessing Damage in Corroded Reinforced Concrete Using Acoustic Emission*, Journal of Engineering Mechanics, **126**(3), pp. 273-283, 2000.

[2] Ohtsu, M. & Tomoda, Y., *Acoustic Emission Techniques for Rebar Corrosion in Reinforced Concrete*, in: Advances in Construction Materials, pp. 615-621, 2007.

[3] Kawasaki, Y., Tomoda Y. & Ohtsu, M., *AE Monitoring of Corrosion Process in Cyclic Wet-Dry Test*, Construction and Building Materials, **24**(12), pp. 2353-2357, 2010.

[4] Ohtsu, M. & Tomoda, Y., *Corrosion Process in Reinforced Concrete Identified by Acoustic Emission*, Materials Transactions, **48**(6), pp. 1184-1189, 2007.

[5] Ohtsu, M. & Tomoda, Y., *Phenomenological Model of Corrosion Process in Reinforced Concrete Identified by Acoustic Emission*, ACI Materials Journal, **105**(2), pp. 194-199, 2008.

[6] Zaki, A., Chai, H.K., Behnia, A., Aggelis, D.G., Tan, J.Y. & Ibrahim, Z, *Monitoring Fracture of Steel Corroded Reinforced Concrete Members Under Flexure by Acoustic Emission Technique*, Construction and Building Materials, **136**, pp. 609-618, 2017.

[7] Zaki, A., Tan, J.Y., Chai, H.K. & Aggelis, D.G., *Assessment of Corrosion Damage using Acoustic Emission Technique under Load Testing*, Proceedings of the 7th Asia Pacific Young Researchers and Graduates Symposium, August 2015.

[8] Kawasaki, Y., Wasada, S., Okamoto, T. & Izuno, K., *Evaluation for RC Specimen Damaged from Rebar Corrosion by Acoustic Emission Technique*, Construction and Building Materials, **67**, pp. 157-164, 2014.

[9] Kawasaki, Y., Wakuda, T., Kobarai, T. & Ohtsu, M., *Corrosion Mechanisms in Reinforced Concrete by Acoustic Emission*, Construction and Building Materials, **48**, pp. 1240-1247, 2013.

[10] Behnia, A., Chai, H.K. & Shiotani, T., *Advanced Structural Health Monitoring of Concrete Structures with the aid of Acoustic Emission*, Construction and Building Materials, **65**, pp. 282-302, 2014.

[11] ElBatanouny, M.K., Ziehl, P.H., Larosche, A., Mangual, J., Matta, F. & Nanni, A., *Acoustic Emission Monitoring for Assessment of Prestressed Concrete Beams*, Construction and Building Materials, **58**, pp. 46-53, 2014.

[12] Behnia, A., Chai, H.K., GhasemiGol, M., Sepehrinezhad, A. & Mousa, A.A., *Advanced Damage Detection Technique by Integration of Unsupervised Clustering into Acoustic Emission*, Engineering Fracture Mechanics, **210**, pp. 212-227, 2019.

[13] GuzmÃ¡n, C., Torres, D., Hucailuk, C. & Filipussi, D., *Analysis of the Acoustic Emission in a Reinforced Concrete Beam Using a Four Points Bending Test*, Procedia Materials Science, **8**, pp. 148-154, 2015.

[14] Aggelis, D.G., Tsangouri, E. & Van Hemelrijck, D., *Influence of Propagation Distance on Cracking and Debonding Acoustic Emissions in Externally Reinforced Concrete Beams*, Meccanica, **50**(5), pp. 1167-1175, 2015.

[15] Leelalerkiet, V., Shimizu, T., Tomoda, Y. & Ohtsu, M., *Estimation of Corrosion in Reinforced Concrete by Electrochemical Techniques and Acoustic Emission*, Journal of Advanced Concrete Technology**, 3**(1), pp. 137-147, 2005.

[16] Behnia, A., Chai, H.K., Yorikawa, M., Momoki, S., Terazawa, M. & Shiotani, T., *Integrated Non-Destructive Assessment of Concrete Structures Under Flexure by Acoustic Emission and Travel Time Tomography*, Construction and Building Materials, **67**(Part B), pp. 202-215, 2014.

[17] Aggelis, D.G., Soulioti, D.V., Sapouridis, N., Barkoula, N.M., Paipetis, A.S. & Matikas, T.E, *Acoustic Emission Characterization of the Fracture Process in Fibre Reinforced Concrete*, Construction and Building Materials, **25**(11), pp. 4126-4131, 2011.

[18] Malhotra, V.M. & Carino, N.J*., CRC Handbook on Nondestructive Testing of Concrete*, CRC Press, 1991.

[19] Ohtsu, M. & Yuyama, S., *Recommended Practice for In-situ Monitoring of Concrete Structures by Acoustic Emission*, Proceeding of 15th International Acoustic Emission Symposium, pp. 263-268, 2000.

[20] Carpinteri, A., Lacidogna, G. & Niccolini, G., *Damage analysis of Reinforced Concrete Buildings by the Acoustic Emission Technique*, Structural Control and Health Monitoring, **18**(6), pp. 660-673, 2011.

[21] Calabrese, L., Campanella, G. & Proverbio, E., *Identification of Corrosion Mechanisms by Univariate and multivariate Statistical Analysis during Long Term Acoustic Emission Monitoring on a pre-Stressed Concrete Beam*, Corrosion Science, **73**, pp. 161-171, 2013.

[22] Van Steen, C., Verstrynge, E., Wevers, M. & Vandewalle, L., *Assessing the Bond Behaviour of Corroded Smooth and Ribbed Rebars with Acoustic Emission Monitoring*, Cement and Concrete Research, **120**, pp. 176-186, 2019.

[23] Ohtsu, M., *Mathematical Theory of Acoustic Emission and Moment Tensor Solution*, Zairyo/Journal of the Society of Materials Science, **36**(408), pp. 1025-1031, 1987.

[24] Colombo, S., Main, I.G. & Forde, M.C., *Assessing Damage of Reinforced Concrete Beam Using 'b-value' Analysis of Acoustic Emission Signals*, Journal of Materials in Civil Engineering, **15(**3), pp. 280-286, 2003.

[25] Grosse, C.U., Reinhardt, H.W. & Finck, F., *Signal-Based Acoustic Emission Techniques in Civil Engineering*, Journal of Materials in Civil Engineering, **15**(3), pp. 274-279, 2003.
[26] Ohno, K. & Ohtsu, M., *Crack Classification in Concrete Based on Acoustic Emission*, Construction and Building Materials, **24**(12), pp. 2339-2346, 2010.
[27] Dunn, S.E., Young, J.D., Hartt, W.H. & Brown, R.P., *Acoustic Emission Characterization of Corrosion Induced Damage in Reinforced Concrete*, Corrosion, **40**(7), pp. 339-343, 1984.
[28] Shiotani, T., Ohtsu, M. & Ikeda, K., *Detection and Evaluation of AE Waves Due to Rock Deformation*, Construction and Building Materials, **15**(5-6), pp. 235-246, 2001.
[29] Nguyen-Tat, T., Ranaivomanana, N. & Balayssac, J.P., *Characterization of Damage in Concrete Beams under Bending with Acoustic Emission Technique (AET)*, Construction and Building Materials, **187**, pp. 487-500, 2018.
[30] ASTM, *ASTM C-610-98A: Definitions of Terms Relating to Acoustic Emission*, American Society of Testing Materials, 1998.
[31] Zaki, A., Chai, H.K., Aggelis, D.G. & Alver, N., *Non-Destructive Evaluation for Corrosion Monitoring in Concrete: A Review and Capability of Acoustic Emission Technique*, Sensors, **15**(8), pp. 19069-19101, 2015.
[32] BS, *BS 4449: Specification Steel for the Reinforcement of Concrete. Weldable Reinforcing Steel. Bar, Coil and Decoiled Product* , British Standards Institution, 2005.
[33] ASTM, ASTM G1-03: *Standard Practice for Preparing, Cleaning, and Evaluating Corrosion Test Specimens*, American Society of Testing Materials, 2003.
[34] BS, *BS 8110-1: Structural Use of Concrete. Code of Practice for Design and Construction*, British Standards Institution, 1997.
[35] Apostolopoulos, C.A. & Michalopoulos, D., *Impact of Corrosion on Mass Loss, Fatigue and Hardness of BSt500s Steel*, Journal of Materials Engineering and Performance, **16**(1), pp. 63-67, 2007.
[36] Majhi, S., Mukherjee, A., George, N.V. & Uy, B., *Corrosion Detection in Steel Bar: A Time-frequency Approach*, NDT & E International, **107**,. 102150, 2019.
[37] Tsangouri, E. & Aggelis, D.G., *A Review of Acoustic Emission as Indicator of Reinforcement Effectiveness in Concrete and Cementitious Composites*, Construction and Building Materials, **224**, pp. 198-205, 2019.